LINC complex branching through structurally diverse SUN-KASH 6:6 assemblies

Authors

Manickam Gurusaran[1] and Owen R. Davies[1]

Affiliations

[1]Biosciences Institute, Faculty of Medical Sciences, Newcastle University, Newcastle upon Tyne NE2 4HH, United Kingdom.

Author for Correspondence

Owen Davies: owen.davies@newcastle.ac.uk

Abstract

The LINC complex mechanically couples cytoskeletal and nuclear components across the nuclear envelope to fulfil a myriad of cellular functions, including nuclear shape and positioning, hearing and meiotic chromosome movements. The canonical model of the LINC complex is of individual linear nucleocytoskeletal linkages provided by 3:3 interactions between SUN and KASH proteins. Here, we provide crystallographic and biophysical evidence that SUN-KASH is a constitutive 6:6 complex in which two SUN trimers interact back-to-back. A common SUN-KASH topology is achieved through structurally diverse 6:6 interaction mechanisms by distinct KASH proteins, including zinc-coordination by Nesprin-4. The SUN-KASH 6:6 complex is incompatible with the current model of a linear LINC complex and instead suggests the formation of a branched LINC complex network. In this model, SUN-KASH 6:6 complexes act as nodes for force distribution and integration between adjacent SUN and KASH molecules, enabling the coordinated transduction of large forces across the nuclear envelope.

Keywords

LINC complex, nuclear envelope, SUN1, Nesprin-4, KASH5, Nesprin-1, X-ray crystallography, small-angle X-ray scattering, biophysics

Introduction

The nuclear envelope partitions nuclear components from the cytoskeleton, thereby necessitating their mechanical coupling across the nuclear envelope to enable cytoskeletal function in the structure and positioning of nuclear contents. This is achieved by the Linker of Nucleoskeleton and Cytoskeleton (LINC) complex, which traverses the nuclear envelope and binds to cytoskeletal and nuclear structures to mediate force transduction between these partitioned components (Starr and Fridolfsson, 2010) (Figure 1a). In this capacity, the LINC complex is essential for cellular life, performing critical functions in nuclear structure, shape and positioning, in addition to tissue-specific functions including sound perception in the inner ear and chromosome movements during meiosis (Lee and Burke, 2018; Meinke and Schirmer, 2015; Starr and Fridolfsson, 2010). Further, mutations of the LINC complex and its interacting partners are associated with human laminopathies, including Hutchison-Gilford progeria syndrome and Emery-Dreifuss muscular dystrophy (Meinke et al., 2011; Mejat and Misteli, 2010).

The LINC complex is formed of SUN (Sad1 and UNC84 homology) domain and KASH (Klarsicht, ANC-1 and Syne homology) domain proteins (Meinke and Schirmer, 2015; Starr and Fridolfsson, 2010), which interact immediately below the outer nuclear membrane, through complex formation between their C-terminal eponymous SUN and KASH domains (Sosa et al., 2012; Wang et al., 2012; Zhou et al., 2012). SUN proteins then traverse the approximately 50 nm peri-nuclear space and cross the inner nuclear membrane, enabling their N-termini to bind to nuclear contents, including reported interactions with the nuclear lamina (Crisp et al., 2006; Haque et al., 2006; Haque et al., 2010), chromatin (Chi et al., 2007) and the telomeric ends of meiotic chromosomes (Shibuya et al., 2014). Similarly, KASH domain proteins cross the outer nuclear membrane and have large cytoplasmic extensions to enable their N-termini to bind to the cytoskeleton (Spindler et al., 2019; Starr and Fridolfsson, 2010). Thus, the LINC complex axis is established by a peri-nuclear SUN-KASH core interaction and mechanically couples the cytoskeleton and nuclear contents (Figure 1a).

In mammals, there are five SUN proteins, of which SUN1 and SUN2 are widely expressed and perform partially redundant functions (Lei et al., 2009; Zhang et al., 2009). There are similarly multiple KASH proteins, four of which are Nesprins (Nuclear Envelope Spectrin Repeat proteins). Nesprin-1 and Nesprin-2 are widely expressed, perform overlapping functions and contain large cytoplasmic spectrin-repeat domains with N-termini that bind to actin (Banerjee et al., 2014; Starr and Fridolfsson, 2010). Nesprin-3 shares a similar KASH domain but its cytoplasmic region binds to plectin, mediating interactions with intermediate filaments (Ketema and Sonnenberg, 2011). The two most divergent KASH proteins, Nesprin-4 and KASH5, exhibit substantial sequence diversity within their KASH domains (Figure 1b). Nesprin-4 functions in the outer hair cells of the inner ear and is essential for hearing (Horn et al., 2013a). Its N-terminus interacts with kinesin, which mediates microtubule binding and plus-end directed movements that achieve the basal positioning of nuclei (Horn et al., 2013a; Roux et al., 2009). KASH5 functions in meiosis and is essential for fertility (Horn et al., 2013b; Morimoto et al., 2012). Its N-terminus interacts with dynein-dynactin (Horn et al., 2013b; Morimoto et al., 2012), which mediates microtubule binding and minus-end directed motility that drives rapid chromosomal movements to facilitate homologous chromosome pairing (Lee et al., 2015; Zetka et al., 2020). Thus, KASH proteins execute a range of LINC complex functions in transmitting actin forces, plus-/minus-end directed microtubule movements and the tensile strength of intermediate filaments into the nucleus.

The canonical model of the LINC complex is based on crystal structures of the SUN-KASH domain complexes formed between SUN2 and Nesprin-1/2 (Sosa et al., 2012; Wang et al., 2012). The SUN domain adopts a 'three-leaf clover'-like structure, in which a globular trimer extends from a short N-terminal trimeric coiled-coil (Sosa et al., 2013). KASH domains are intertwined between SUN protomers and their path is defined by three distinct regions. The KASH C-terminus contains a triple proline motif that packs between the globular cores of SUN protomers. The KASH mid-region winds around the trimeric arc and is wedged between the globular core of one SUN protomer and a β-turn-β loop, known as the KASH-lid, of the adjacent protomer. The KASH N-terminus then turns by >90˚ to

radiate out from the trimer axis and forms a disulphide bond with a SUN protomer (between SUN2 and KASH1 amino-acids C563 and C8774, respectively), which is predicted to enhance the tensile strength of SUN-KASH (Jahed et al., 2015; Sosa et al., 2012). The biological unit of SUN-KASH was interpreted from the crystal lattice as a 3:3 complex, comprising three KASH domains bound to a single SUN trimer (Sosa et al., 2012; Wang et al., 2012). On this basis, it was proposed that the LINC complex consists of a SUN-KASH 3:3 complex that is orientated vertically to allow KASH proteins to cross the outer nuclear membrane and SUN to form an extended trimeric coiled-coil that spans the peri-nuclear space (Sosa et al., 2013; Sosa et al., 2012) (Figure 1a). Thus, the canonical model of the LINC complex is of individual linear structures that provide independent nucleocytoskeletal couplings. Whilst it has been proposed that branching or higher-order assembly between LINC complexes may be advantageous in distributing large forces and achieving coordinated motions (Jahed et al., 2018; Lu et al., 2008; Sosa et al., 2013; Wang et al., 2012; Zhou et al., 2012), we have hitherto lacked structural evidence in favour of this hypothesis.

Here, we provide crystallographic and biophysical evidence in support of the LINC complex forming a branched network rather than individual linear structures. We find that SUN-KASH complexes between SUN1 and Nesprin-4, KASH5 and Nesprin-1 are 6:6 structures that consist of constitutive back-to-back interactions between SUN trimers. The three distinct KASH domains provide structurally diverse but related 6:6 interfaces that achieve the same topology with potential hinge-like motion between SUN trimers. The SUN-KASH 6:6 complex is incompatible with the current model of a linear LINC complex, and instead suggests the formation of a branched LINC complex network. Thus, we propose that SUN-KASH domain complexes act as nodes for branching and integration between LINC complexes to achieve the coordinated transduction of large forces across the nuclear envelope.

Results

SUN-KASH complexes are 6:6 hetero-oligomers

The previously reported crystal structures of SUN-KASH complexes between SUN2 and Nesprins 1-2 revealed almost identical structures that were interpreted as 3:3 hetero-oligomers (Sosa et al., 2012; Wang et al., 2012). The KASH domains of Nesprin-4 and KASH5 exhibit sequence divergence from Nesprins 1-3, including the presence of conserved N-terminal motifs of 381-CCSH-384 and 545-PPP-547, respectively (Figure 1b). On this basis, we reasoned that Nesprin-4 and KASH5 may impose unique SUN-KASH structures that differ from the classical architecture of Nesprin 1-3 complexes, which may underlie their specialised functional roles. We thus solved the X-ray crystal structures of SUN-KASH complexes formed between the SUN domain of SUN1 and KASH domains of Nesprin-4 and KASH5 (herein referred to as SUN1-KASH4 and SUN1-KASH5). The SUN1-KASH4 structure was solved at a resolution of 2.75 Å and revealed a 6:6 assembly in which two globular 3:3 complexes are held in a back-to-back configuration through zinc-coordination by opposing KASH4 molecules across the 6:6 interface (Figure 1c, Table 1 and Supplementary Figure 1a,b). The SUN1-KASH5 crystal structure was solved at 1.54 Å resolution and revealed a similar 6:6 assembly in which opposing 3:3 complexes are held together by extensive interactions between opposing KASH5 molecules and KASH-lids (Figure 1c, Table 1 and Supplementary Figure 1a,c). Thus, both Nesprin-4 and KASH5 form SUN-KASH 6:6 hetero-oligomers in which similar topologies of back-to-back 3:3 complexes are achieved through structurally diverse 6:6 interfaces.

Is the 6:6 assembly unique to SUN-KASH complexes formed by Nesprin-4 and KASH5? We next solved the crystal structure of the SUN-KASH complex between SUN1 and Nesprin-1 (herein referred to as SUN1-KASH1). The SUN1-KASH1 structure was solved at 1.82 Å resolution and demonstrated a similar 6:6 back-to-back assembly, albeit with less extensive interface-spanning interactions provided solely by opposing KASH-lids (Figure 1c, Table 1 and Supplementary Figure 1a,d). Importantly, the SUN1-KASH1 structure closely matches the previous SUN2-KASH1/2 structures, in which similar 6:6

interfaces were present in the crystal lattice but were dismissed as crystal contacts (Supplementary Figure 1e) (Sosa et al., 2012; Wang et al., 2012). It was thus critical to determine whether SUN1-KASH1 is a 6:6 complex in solution. We utilised size-exclusion chromatography multi-angle light scattering (SEC-MALS) as the gold standard for determining molecular species. SEC-MALS revealed that all SUN-KASH complexes are 6:6 hetero-oligomers (Figure 1d and Supplementary Figure 2a). Moreover, their 6:6 complexes remained intact at the lowest detectable concentration (Supplementary Figure 2b-d) and we failed to detect 3:3 complexes in any biochemical conditions tested. Thus, we conclude that SUN-KASH complexes are 6:6 hetero-oligomers in which two 3:3 complexes interact in back-to-back configurations. The SUN-KASH 6:6 structure is incompatible with the current model of a linear LINC complex and instead demonstrates a constitutive interaction between SUN trimers that mediates the physical coupling of adjacent LINC complexes within the peri-nuclear space.

Structural diversity within the SUN-KASH 6:6 interface

Our SUN-KASH crystal structures reveal the formation of similar 6:6 architectures through diverse back-to-back interfaces. Whilst the C-termini of all three KASH domains adopt the same structure, their N-termini differ substantially (Figure 2a,b). KASH1 undergoes a turn of >90˚ to radiate from the trimer axis, similar to the previously reported SUN2-KASH1/2 structures (Supplementary Figure 1e), whereas KASH4 and KASH5 follow the arc of the SUN1 trimer, enabling them to contribute directly to the 6:6 interface (Figure 2a,b).

SUN1-KASH4 adopts an unusual conformation in which the 6:6 complex is held together by three interface spanning zinc-sites, each coordinated by opposing KASH4 molecules (Figure 2c and Supplementary Figure 3a). The presence of metal ions in the crystal structure was confirmed by corresponding peaks in anomalous difference electron density maps (Figure 2d), and their identity as zinc ions that were co-purified from bacterial expression was confirmed by the spectrophotometric determination of three zinc ions per 6:6 complex in solution that were lost upon pre-incubation with

EDTA (Figure 2e). The zinc-sites are coordinated by asymmetric ligands from 381-CCSH-384 motifs of opposing KASH4 molecules, comprising C381 and C382 from one molecule, and C382 and H384 from the other (Figure 2c), and mutation of both cysteine residues to serine was sufficient to preclude zinc-binding (Figure 2e). The three zinc-sites form a tripod of interactions that provide the sole interface-spanning contacts between opposing 3:3 complexes (Figure 2b).

SUN1-KASH5 demonstrates the most extensive 6:6 interface in which KASH5 molecules and SUN1 KASH-lids from opposing 3:3 complexes wind around each other in a right-handed screw to create a complete circumferential interface enclosing a hollow core, similar to a β-barrel fold (Figure 2f and Supplementary Figure 3b). KASH5 follows an almost linear path, packed between a SUN1 globular core and KASH-lids of opposing SUN1 protomers, with N-terminal 545-PPP-547 motifs of opposing molecules interacting across the interface. KASH5 and KASH4 follow similar paths, with KASH5 PPP-motif interactions and KASH4 zinc-sites located at the same positions and providing analogous interface-spanning interactions (Figure 2a,b). However, an important distinction is that a torsional rotation of approximately 20˚ between the 3:3 complexes of SUN1-KASH5, relative to SUN1-KASH4, brings together opposing KASH-lids and enables their interaction across the interface (Figure 2f). Thus, tip-to-tip interactions via amino-acids I673 and F671 of opposing SUN1 KASH-lids contribute to the extensive 6:6 interface of SUN1-KASH5 (Figure 2f).

The SUN1-KASH1 6:6 complex is formed solely of a tripod of KASH-lid tip-to-tip interactions mediated by amino-acids I673 and F671, in the same manner and owing to the same torsional rotation as in the SUN1-KASH5 structure (Figure 2g and Supplementary Figure 3c). KASH1 undergoes acute angulation away from the 6:6 interface (Figure 2a,b), as previously observed in SUN2-KASH1/2 (Supplementary Figure 1e). As such, whilst amino-acid F8784 binds to the KASH-lids of each tip-to-tip interaction site (Figure 2g), KASH1's N-terminus does not contribute to the 6:6 interface (Figure 2a,b). This creates an open interface, with large solvent channels between opposing 3:3 complexes (Supplementary Figure

3c). Overall, the three structures demonstrate alternative SUN-KASH 6:6 interaction mechanisms that are differentially exploited by KASH proteins. SUN1-KASH4 and SUN1-KASH1 represent extreme states of this spectrum in which the 6:6 interface is mediated solely by KASH-mediated metal coordination and SUN1 KASH-lids, respectively. In contrast, SUN1-KASH5 adopts an intermediate structure that utilises both KASH and KASH-lid interaction mechanisms to form a fully enclosed 6:6 interface.

SUN1-KASH1 complex formation depends on KASH-lid 6:6 interactions

On the basis of their crystal structures, we predicted that KASH-lid tip-to-tip interactions are essential for 6:6 hetero-oligomer formation in solution by SUN1-KASH1 but not SUN1-KASH4. We tested this by generating glutamate mutations of KASH-lid tip amino-acids I673 and F671, which mediate interface-spanning tip-to-tip interactions within SUN1-KASH1 and SUN1-KASH5 but have no contacts within their respective 3:3 complexes (Figure 2c,f,g and Supplementary Figure 4a-c). We also analysed a glutamate mutation of amino-acid W676, which mediates hydrophobic interactions with the KASH domain within a constituent 3:3 complex (Supplementary Figure 4a-c), and acted as a negative control in disrupting all three SUN-KASH complexes (Figure 3a,b).

The SUN1-KASH4 6:6 complex was impervious to KASH-lid mutations I673E and F671E (Figure 3a,b and Supplementary Figure 4d,e), in keeping with the lack of KASH-lid tip-to-tip interactions at its 6:6 interface. In stark contrast, SUN1-KASH1 was disrupted by I673E and F671E mutations (Figure 3a,b and Supplementary Figure 4d), confirming that KASH-lid tip-to-tip interactions are essential for its 6:6 complex formation. The dissociated SUN1 I673E protein was monomeric, similar to wild-type SUN1 expressed in absence of a KASH domain (Supplementary Figure 5a), and SAXS analysis confirmed that its SUN domain remained folded (Supplementary Figure 5b-f and Table 2). The failure to observe smaller hetero-oligomers demonstrates that SUN1-KASH1 3:3 complexes are unstable in absence of the 6:6 interface, indicating that SUN1-KASH1 is a constitutive 6:6 hetero-oligomer. In agreement with the equal roles of KASH domain and KASH-lid interactions at its 6:6 interface, SUN1-KASH5 exhibited

intermediate phenotypes upon I673E and F671E mutation, with retention of complex formation but reduction in oligomer size to species that likely reflect partially dissociating 6:6 complexes (Figure 3a,b and Supplementary Figure 4d,e). We conclude that the diverse roles of KASH-lids at the 6:6 interfaces of SUN-KASH crystal structures are truly reflective of their solutions states and that KASH-lid tip-to-tip interactions are essential for assembly of a constitutive SUN1-KASH1 6:6 hetero-oligomer.

Hinge-like motion of the SUN-KASH 6:6 interface

How is the SUN-KASH 6:6 complex orientated within the nuclear envelope? Its back-to-back assembly suggests a horizontal orientation, parallel to the outer nuclear membrane, with SUN trimers organised obliquely within the peri-nuclear space. In this configuration, tension forces carried by SUN and KASH molecules would exert bending moments on the structure, favouring a hinge-like angulation between opposing 3:3 complexes. We thus utilised small-angle X-ray scattering (SAXS) to determine whether SUN-KASH complexes adopt angled conformations in solution. Whilst SAXS data of SUN1-KASH4 and SUN1-KASH5 were closely fitted by their crystal structures upon flexible modelling of missing termini (χ^2 values of 1.25 and 1.70), we achieved only poor fits for SUN1-KASH1 (χ^2 = 4.83) (Supplementary Figure 6a-c and Table 2). In case of large-scale motion, we performed SAXS-based rigid-body modelling using two SUN1-KASH1 3:3 complexes as independent rigid bodies. We consistently obtained models that closely fitted experimental data (χ^2 = 1.56) in which 3:3 complexes interact back-to-back with a bend of approximately 60˚ relative to the crystal structure (Figure 4a, Supplementary Figure 6a,d and Table 2). In this model, two pairs of KASH-lid tip-to-tip interactions by I673 and F671 are retained, whilst the third is disrupted, and an additional interface is formed between opposing central KASH-lids. Thus, KASH-lids act as a hinge at the 6:6 interface, opening the linear crystal structure into an angled conformation that is seemingly more stable in solution. This hinged structure is suited to force transduction between oblique SUN and KASH molecules and places all six KASH1 N-termini in favourable positions to cross the outer nuclear membrane.

Is a similar hinge-like angulation possible for SUN1-KASH4 and SUN1-KASH5? Whilst their extensive 6:6 interfaces retain linear structure in solution (Supplementary Figure 6a-c and Table 2), angulation may be achieved by tension forces. We thus performed normal mode analysis to determine whether angled structures are conformationally accessible. We observed low frequency normal modes corresponding to hinge-like angulation at the 6:6 interface for all SUN-KASH complexes (Figure 4b), indicating that angled conformations are accessible flexible states. We thus conclude a model in which hinged SUN-KASH 6:6 complexes, parallel with the outer nuclear membrane, act as nodes for the integration and distribution of tension forces between oblique SUN trimers and KASH molecules within a branched LINC complex network (Figure 5).

Discussion

The LINC complex is essential for nuclear shape and positioning in almost all eukaryotic cells, and fulfils a number of specialised roles, such as in hearing and meiotic cell division (Lee and Burke, 2018; Meinke and Schirmer, 2015; Starr and Fridolfsson, 2010). As a mechanical transducer, the structure-function relationship underlies the highly diverse cellular roles of the LINC complex. Specifically, the structure and oligomeric assembly of its protein components dictate the topology of the LINC complex and thereby its mechanism of force transduction within the nuclear envelope. On the basis of their X-ray crystal structures and solution states, we report that the globular SUN-KASH cores of diverse LINC complexes are constitutive 6:6 hetero-oligomers in which SUN trimers interact back-to-back. This topology is incompatible with the current model of individual linear 3:3 LINC complexes (Sosa et al., 2013; Sosa et al., 2012), and instead indicates the formation of a branched LINC complex network.

A branched network is an attractive means for force transduction as it can transmit forces of magnitudes far in excess of those carried by single molecules, is impervious to disruption of individual linkages, and allows communication and coordination between adjacent molecules. Thus, SUN-KASH 6:6 hetero-oligomers enable force distribution and integration between adjacent molecules to achieve coordinated actions within the nucleus. In this capacity, LINC complex branching by SUN-KASH 6:6 assembly explains previous cellular observations of higher-order LINC complex structures, including its immobility within the nuclear envelope (Lu et al., 2008), foci formation within the meiotic nuclear envelope (Ding et al., 2007; Horn et al., 2013b; Morimoto et al., 2012), and the formation of transmembrane actin-associated nuclear (TAN) lines (Luxton et al., 2010).

The back-to-back nature of SUN-KASH 6:6 complexes suggests their orientation parallel to the outer nuclear membrane, with SUN trimers organised obliquely within the peri-nuclear space (Figure 5). Our SAXS analysis of SUN1-KASH1 indicates that it adopts a hinged conformation in solution, stabilised by two KASH-lid tip-to-tip interactions and the lateral association of central KASH-lids. This provides a

more extensive interface than the tripod of KASH-lid tip-to-tip interactions within the crystal structure, explaining its preferential formation outside of a crystal lattice. In contrast, SUN1-KASH4 and SUN1-KASH5 have extensive 6:6 interfaces that preserve linearity in solution. Nevertheless, normal mode analysis predicted that hinged structures of all three SUN-KASH complexes are conformationally accessible states. Thus, SUN-KASH 6:6 hetero-oligomers may become angled in response to tension forces carried by obliquely orientated SUN and KASH molecules. All three SUN-KASH 6:6 interfaces consist of circumferential exteriors and hollow cores that are largely hydrophobic in nature. Thus, we envisage that the SUN-KASH hinged structure may be stabilised by interaction of its 6:6 interface with phospholipids of the outer nuclear membrane, potentially forming an integrated membrane-bound complex between a 6:6 hetero-oligomer and the transmembrane regions of its six KASH proteins.

How do the diverse 6:6 interfaces provided by KASH proteins facilitate their specialised functions? An intriguing observation is that Nesprin-4 and KASH5, which transduce microtubule forces (Horn et al., 2013a; Horn et al., 2013b; Morimoto et al., 2012; Roux et al., 2009), demonstrate extensive interactions at their 6:6 interfaces. In contrast, a far less extensive 6:6 interface is found in classical Nesprins, which transduce actin forces and the tensile strength of intermediate filaments (Banerjee et al., 2014; Ketema and Sonnenberg, 2011; Starr and Fridolfsson, 2010). Thus, cytoskeletal components may have differential requirements for the strength, structure and stability of SUN-KASH 6:6 hetero-oligomers. Further, their diverse interfaces may provide disparate mechanisms for the timely assembly and disassembly of LINC complex networks during miotic and meiotic cell cycles. This could be achieved by inhibition of the 6:6 interface, which is sufficient to disrupt the SUN1-KASH1 globular complex. Further, as the SUN1-KASH4 6:6 interface is mediated by zinc-coordination sites, its formation could be regulated by zinc availability and sequestration within the peri-nuclear space.

The SUN-KASH 6:6 hetero-oligomer provides the first structural evidence, but perhaps not the sole structural means, of LINC complex network formation. Additional branching events could result from

variation in oligomer state along the SUN-KASH axis. Whilst SUN is assumed to form a trimeric coiled-coil extending from its globular core, its protein sequence is inconsistent with formation of a single continuous coiled-coil. Instead, it suggests the presence of short discrete coiled-coils, of potentially distinct oligomers, that are connected by unstructured linkers. Further, C526 residues of SUN1 are reported to form disulphide bonds (Lu et al., 2008), suggesting tethering between SUN trimers from separate SUN-KASH 6:6 complexes. Thus, oligomer variation and disulphide formation may combine with the SUN-KASH 6:6 interface to provide multiple branching events within the peri-nuclear space. Whilst there is no reported structural information regarding KASH proteins, we find that KASH5 is dimeric (Manickam & Davies, unpublished findings), indicating branching between SUN-KASH 6:6 complexes and their cytoskeletal attachments. Thus, we propose that coordinated force transduction is achieved by a highly branched LINC complex network. In this model, the lowest degree of branching supported by current structural evidence is of SUN-KASH 6:6 hetero-oligomers mediating force distribution and integration between three KASH dimers and two SUN trimers (Figure 5).

Methods

Recombinant protein expression and purification

The SUN domain of human SUN1 (amino-acid residues 616-812) was fused to an N-terminal TEV-cleavable His_6-GCN4 tag (as described in Sosa et al. (2012)) and cloned into a pRSF-Duet1 (Merck Millipore) vector. The KASH domains of human KASH5 (amino-acid residues 542-582), Nesprin-4 (KASH4, amino-acid residues 376-404) and Nesprin-1 (KASH1, amino-acid residues 8769-8797) were cloned into pMAT11 (Peranen et al., 1996) vectors for expression as TEV-cleavable His_6-MBP fusion proteins respectively. SUN1 and KASH constructs were co-expressed in BL21 (DE3) cells (Novagen®), in 2xYT media, induced with 0.5 mM IPTG for 16 hours at 25°C. Cell disruption was achieved by sonication in 20 mM Tris pH 8.0, 500 mM KCl and cellular debris removed by centrifugation at 40,000 g. Fusion proteins were purified through consecutive Ni-NTA (Qiagen), amylose (NEB), and HiTrap Q HP (GE Healthcare) ion exchange chromatography. TEV protease was utilised to remove affinity tags and cleaved samples were purified through ion exchange chromatography and size exclusion chromatography (HiLoad™ 16/600 Superdex 200, GE Healthcare) in 20 mM Tris pH 8.0, 150 mM KCl, 2 mM DTT. Protein samples were concentrated using Microsep™ Advance Centrifugal Devices 10,000 MWCO centrifugal filter units (PALL) and were stored at -80˚C following flash-freezing in liquid nitrogen. Protein samples were analysed by SDS-PAGE and visualised with Coomassie staining. Concentrations were determined by UV spectroscopy using a Cary 60 UV spectrophotometer (Agilent) with extinction coefficients and molecular weights calculated by ProtParam (http://web.expasy.org/protparam/).

Crystal structure solution of SUN1-KASH4 (PDB accession 6R16)

SUN1-KASH4 protein crystals were obtained through vapour diffusion in sitting drops, by mixing 100 nl of protein at 25 mg/ml with 100 nl of crystallisation solution (0.06 M $MgCl_2$; 0.06 M $CaCl_2$; 0.1 M Imidazole pH 6.5; 0.1M MES (acid) pH 6.5; 18% Ethylene glycol; 18% PEG 8K) and equilibrating at 20°C for 4-9 days. Crystals were flash frozen in liquid nitrogen. X-ray diffraction data were collected at

0.9795 Å, 100 K, as 2000 consecutive 0.10° frames of 0.040 s exposure on a Pilatus 6M-F detector at beamline I04 of the Diamond Light Source synchrotron facility (Oxfordshire, UK). Data were indexed and integrated in XDS (Kabsch, 2010), scaled in XSCALE (Diederichs et al., 2003) and merged using Aimless (Evans, 2011). Crystals belong to orthorhombic spacegroup $P2_12_12_1$ (cell dimensions a = 104.37 Å, b = 117.21 Å, c = 138.42 Å, α = 90°, β = 90°, γ = 90°), with six copies of SUN1 and KASH4 per asymmetric unit. The structure was solved by molecular replacement using Phaser (McCoy et al., 2007), with SUN1-KASH1 (this study, PDB accession 6R15) as a search model. The structure was re-built by PHENIX Autobuild (Adams et al., 2010) and completed through iterative manual model building in Coot (Emsley et al., 2010), with the addition of six potassium ions, three zinc ions and ethylene glycol ligands. The structure was refined using PHENIX refine (Adams et al., 2010) with isotropic atomic displacement parameters and TLS parameters, using SUN1-KASH1 as a reference structure. The structure was refined against 2.75 Å data to R and R_{free} values of 0.2190 and 0.2549 respectively, with 98.22% of residues within the favoured regions of the Ramachandran plot (0 outliers), clashscore of 4.89 and overall MolProbity score of 1.26 (Chen et al., 2010). The final SUN1-KASH4 model was analysed using the *Online_DPI* webserver (http://cluster.physics.iisc.ernet.in/dpi) to determine a Cruikshank diffraction precision index (DPI) of 0.25 Å (Kumar et al., 2015).

Crystal structure solution of SUN1-KASH5 (PDB accession 6R2I)

SUN1-KASH5 protein crystals were obtained through vapour diffusion in sitting drops, by mixing 100 nl of protein at 25 mg/ml with 100 nl of crystallisation solution (0.12 M 1,6-Hexanediol; 0.12 M 1-Butanol 1,2-Propanediol (racemic); 0.12 M 2-Propanol; 0.12 M 1,4-Butanediol; 0.12 M 1,3-Propanediol; 0.1 M Imidazole pH 6.5 ; 0.1 M MES (acid) pH 6.5; 18% Glycerol; 18% PEG 4K) and equilibrating at 20°C for 4-9 days. Crystals were flash frozen in liquid nitrogen. X-ray diffraction data were collected at 0.9282 Å, 100 K, as 2000 consecutive 0.10° frames of 0.050 s exposure on a Pilatus 6M-F detector at beamline I04-1 of the Diamond Light Source synchrotron facility (Oxfordshire, UK). Data were indexed, integrated, scaled and merged in AutoPROC using XDS (Kabsch, 2010) and Aimless

(Evans, 2011). Crystals belong to hexagonal spacegroup $P6_322$ (cell dimensions a = 80.16 Å, b = 80.16 Å, c = 177.62 Å, α = 90°, β = 90°, γ = 120°), with one copy of SUN1 and KASH5 per asymmetric unit. The structure was solved by molecular replacement using Phaser (McCoy et al., 2007), with SUN1-KASH1 (this study, PDB accession 6R15) as a search model. The structure was re-built by PHENIX Autobuild (Adams et al., 2010) and completed through iterative manual model building in Coot (Emsley et al., 2010), with the addition of a potassium ion. The structure was refined using PHENIX refine (Adams et al., 2010), using anisotropic atomic displacement parameters. The structure was refined against 1.54 Å data to R and R_{free} values of 0.1495 and 0.1683, respectively, with 96.71% of residues within the favoured regions of the Ramachandran plot (0 outliers), clashscore of 6.11 and overall MolProbity score of 1.54 (Chen et al., 2010). The final SUN1-KASH5 model was analysed using the *Online_DPI* webserver (http://cluster.physics.iisc.ernet.in/dpi) to determine a Cruikshank diffraction precision index (DPI) of 0.06 Å (Kumar et al., 2015).

Crystal structure solution of SUN1-KASH1 (PDB accession 6R15)

SUN1-KASH1 protein crystals were obtained through vapour diffusion in sitting drops, by mixing 100 nl of protein at 21 mg/ml with 100 nl of crystallisation solution (0.09 M NaF; 0.09 M NaBr; 0.09 M NaI; 0.1M Sodium HEPES pH 7.5; 0.1 M MOPS (acid) pH 7.5; 18% PEGMME 550; 18% PEG 20K) and equilibrating at 20°C for 4-9 days. Crystals were flash frozen in liquid nitrogen. X-ray diffraction data were collected at 0.9282 Å, 100 K, as 2000 consecutive 0.10° frames of 0.100 s exposure on a Pilatus 6M-F detector at beamline I04-1 of the Diamond Light Source synchrotron facility (Oxfordshire, UK). Data were indexed, integrated, scaled and merged in Xia2 (Winter, 2010) using XDS (Kabsch, 2010), XSCALE (Diederichs et al., 2003) and Aimless (Evans, 2011). Crystals belong to hexagonal spacegroup $P6_322$ (cell dimensions a = 80.45 Å, b = 80.45 Å, c = 182.55 Å, α = 90°, β = 90°, γ = 120°), with one copy of SUN1 and KASH1 per asymmetric unit. The structure was solved by molecular replacement using Phaser (McCoy et al., 2007), with SUN2-KASH1 (PDB accession 4DXR) (Sosa et al., 2012) as a search model. The structure was re-built by PHENIX Autobuild (Adams et al., 2010) and completed through

iterative manual model building in Coot (Emsley et al., 2010), with the addition of a potassium ion, and PEG and HEPES ligands. The structure was refined using PHENIX refine (Adams et al., 2010), using isotropic atomic displacement parameters with four TLS groups per chain. The structure was refined against 1.82 Å data to R and R_{free} values of 0.1587 and 0.1817, respectively, with 96.86% of residues within the favoured regions of the Ramachandran plot (0 outliers), clashscore of 0.00 and overall MolProbity score of 0.69 (Chen et al., 2010). The final SUN1-KASH1 model was analysed using the *Online_DPI* webserver (http://cluster.physics.iisc.ernet.in/dpi) to determine a Cruikshank diffraction precision index (DPI) of 0.06 Å (Kumar et al., 2015).

Size-exclusion chromatography multi-angle light scattering (SEC-MALS)

The absolute molar masses of protein samples and complexes were determined by size-exclusion chromatography multi-angle light scattering (SEC-MALS). Protein samples at >1 mg/ml (unless otherwise states) were loaded onto a Superdex™ 200 Increase 10/300 GL size exclusion chromatography column (GE Healthcare) in 20 mM Tris pH 8.0, 150 mM KCl, 2 mM DTT, at 0.5 ml/min using an ÄKTA™ Pure (GE Healthcare). The column outlet was fed into a DAWN® HELEOS™ II MALS detector (Wyatt Technology), followed by an Optilab® T-rEX™ differential refractometer (Wyatt Technology). Light scattering and differential refractive index data were collected and analysed using ASTRA® 6 software (Wyatt Technology). Molecular weights and estimated errors were calculated across eluted peaks by extrapolation from Zimm plots using a dn/dc value of 0.1850 ml/g. SEC-MALS data are presented as differential refractive index (dRI) profiles with fitted molecular weights (M_W) plotted across elution peaks.

Spectrophotometric determination of zinc content

The presence of zinc in protein samples was determined through a spectrophotometric method using the metallochromic indicator 4-(2-pyridylazo) resorcinol (PAR) (Sabel et al., 2009). Protein samples at 90-200 µM, corresponding to SUN1-KASH4 wild-type and CC381/382SS, and a wild-type sample that

had been treated with EDTA prior to gel-filtration, were digested with 0.6 µg/µl proteinase K (NEB) at 60°C for 1 hour. 10 µl of the supernatant of each protein digestion was added to 80 µl of 50 µM 4-(2-pyridylazo)-resorcinol (PAR) in 20 mM Tris, pH 8.0, 150 mM KCl, incubated for 5 min at room temperature, and UV absorbance spectra were recorded between 600 and 300 nm (Varian Cary 60 spectrophotometer). Zinc concentrations were estimated from the ratio between absorbance at 492 and 414 nm, plotted on a line of best fit obtained from analysis of 0–100 µM zinc acetate standards.

KASH-binding by SUN1 point mutants

The wild-type and individual point mutations I673E, F671E and W676E of SUN1 (as His_6-GCN4 fusions) were co-expressed with KASH (as His_6-MBP fusion) as described above. Initial purification was performed by amylose affinity chromatography (NEB), relying on the residual affinity of SUN1 in cases when point mutations were disruptive. Resultant protein mixtures were analysed by ion exchange chromatography using HiTrap Q HP (GE Healthcare) and comparable samples from full elution profiles of wild-type and mutant proteins for each KASH binding-partner were analysed by SDS-PAGE. The entire elutions were then pooled, concentrated and analysed by size-exclusion chromatography on a Superdex™ 200 Increase 10/300 GL size exclusion chromatography column (GE Healthcare) in 20 mM Tris pH 8.0, 150 mM KCl, 2 mM DTT, at 0.5 ml/min using an ÄKTA™ Pure (GE Healthcare). Elution fractions of wild-type and mutant proteins for each KASH binding-partner were analysed by SDS-PAGE.

Size-exclusion chromatography small-angle X-ray scattering (SEC-SAXS)

SEC-SAXS experiments were performed at beamline B21 of the Diamond Light Source synchrotron facility (Oxfordshire, UK). Protein samples at concentrations >10 mg/ml were loaded onto a Superdex™ 200 Increase 10/300 GL size exclusion chromatography column (GE Healthcare) in 20 mM Tris pH 8.0, 150 mM KCl at 0.5 ml/min using an Agilent 1200 HPLC system. The column outlet was fed into the experimental cell, and SAXS data were recorded at 12.4 keV, detector distance 4.014 m, in 3.0 s frames. ScÅtter 3.0 (http://www.bioisis.net) was used to subtract, average the frames and carry

out the Guinier analysis for the radius of gyration (*Rg*), and *P(r)* distributions were fitted using *PRIMUS* (P.V.Konarev, 2003). *Ab initio* modelling was performed using *DAMMIF* (Franke and Svergun, 2009); 30 independent runs were performed in P1 and averaged. Crystal structures and models were fitted to experimental data using *CRYSOL* (Svergun D.I., 1995). Normal mode analysis was used to model conformational flexibility for fitting to SAXS data using *SREFLEX* (Panjkovich and Svergun, 2016), and rigid body and flexible termini modelling was performed using *CORAL* (Petoukhov et al., 2012).

Normal mode analysis of SUN1-KASH structures

Non-linear normal modes were calculated and visualised for SUN1-KASH 6:6 structures using the NOLB algorithm (Hoffmann and Grudinin, 2017) within the normal mode analysis SAMSON element (https://www.samson-connect.net).

Protein sequence and structure analysis

Nesprin sequences were aligned and visualised using MUSCLE (Madeira et al., 2019) and Jalview (Waterhouse et al., 2009). Molecular structure images were generated using the PyMOL Molecular Graphics System, Version 2.3 Schrödinger, LLC.

Data availability

Crystallographic structure factors and atomic coordinates have been deposited in the Protein Data Bank (PDB) under accession numbers 6R15, 6R16 and 6R2I. All other data are available from the corresponding author upon reasonable request.

Acknowledgements

We thank Diamond Light Source and the staff of beamlines I04, I04-1 and B21 (proposals mx13587, mx18598 and sm15836), A. Basle for assistance with X-ray crystallographic data collection, and J. Dunce for critically reviewing the manuscript. O.R.D. is a Sir Henry Dale Fellow jointly funded by the Wellcome Trust and Royal Society (Grant Number 104158/Z/14/Z).

Author contributions

M.G. performed all experimental work. O.R.D. designed experiments, analysed data and wrote the manuscript.

Competing financial interests

The authors declare no competing interests.

References

Adams, P.D., Afonine, P.V., Bunkoczi, G., Chen, V.B., Davis, I.W., Echols, N., Headd, J.J., Hung, L.W., Kapral, G.J., Grosse-Kunstleve, R.W.*, et al.* (2010). PHENIX: a comprehensive Python-based system for macromolecular structure solution. Acta Crystallogr D Biol Crystallogr *66*, 213-221.

Banerjee, I., Zhang, J., Moore-Morris, T., Pfeiffer, E., Buchholz, K.S., Liu, A., Ouyang, K., Stroud, M.J., Gerace, L., Evans, S.M.*, et al.* (2014). Targeted ablation of nesprin 1 and nesprin 2 from murine myocardium results in cardiomyopathy, altered nuclear morphology and inhibition of the biomechanical gene response. PLoS Genet *10*, e1004114.

Chen, V.B., Arendall, W.B., Headd, J.J., Keedy, D.A., Immormino, R.M., Kapral, G.J., Murray, L.W., Richardson, J.S., and Richardson, D.C. (2010). MolProbity: all-atom structure validation for macromolecular crystallography. Acta Crystallogr D *66*, 12-21.

Chi, Y.H., Haller, K., Peloponese, J.M., Jr., and Jeang, K.T. (2007). Histone acetyltransferase hALP and nuclear membrane protein hsSUN1 function in de-condensation of mitotic chromosomes. J Biol Chem *282*, 27447-27458.

Crisp, M., Liu, Q., Roux, K., Rattner, J.B., Shanahan, C., Burke, B., Stahl, P.D., and Hodzic, D. (2006). Coupling of the nucleus and cytoplasm: role of the LINC complex. J Cell Biol *172*, 41-53.

Diederichs, K., McSweeney, S., and Ravelli, R.B. (2003). Zero-dose extrapolation as part of macromolecular synchrotron data reduction. Acta Crystallogr D Biol Crystallogr *59*, 903-909.

Ding, X., Xu, R., Yu, J., Xu, T., Zhuang, Y., and Han, M. (2007). SUN1 is required for telomere attachment to nuclear envelope and gametogenesis in mice. Developmental cell *12*, 863-872.

Emsley, P., Lohkamp, B., Scott, W.G., and Cowtan, K. (2010). Features and development of Coot. Acta Crystallogr D Biol Crystallogr *66*, 486-501.

Evans, P.R. (2011). An introduction to data reduction: space-group determination, scaling and intensity statistics. Acta Crystallogr D Biol Crystallogr *67*, 282-292.

Franke, D., and Svergun, D.I. (2009). DAMMIF, a program for rapid ab-initio shape determination in small-angle scattering. Journal of applied crystallography *42*, 342-346.

Haque, F., Lloyd, D.J., Smallwood, D.T., Dent, C.L., Shanahan, C.M., Fry, A.M., Trembath, R.C., and Shackleton, S. (2006). SUN1 interacts with nuclear lamin A and cytoplasmic nesprins to provide a physical connection between the nuclear lamina and the cytoskeleton. Mol Cell Biol *26*, 3738-3751.

Haque, F., Mazzeo, D., Patel, J.T., Smallwood, D.T., Ellis, J.A., Shanahan, C.M., and Shackleton, S. (2010). Mammalian SUN protein interaction networks at the inner nuclear membrane and their role in laminopathy disease processes. J Biol Chem *285*, 3487-3498.

Hoffmann, A., and Grudinin, S. (2017). NOLB: Nonlinear Rigid Block Normal-Mode Analysis Method. J Chem Theory Comput *13*, 2123-2134.

Horn, H.F., Brownstein, Z., Lenz, D.R., Shivatzki, S., Dror, A.A., Dagan-Rosenfeld, O., Friedman, L.M., Roux, K.J., Kozlov, S., Jeang, K.T.*, et al.* (2013a). The LINC complex is essential for hearing. J Clin Invest *123*, 740-750.

Horn, H.F., Kim, D.I., Wright, G.D., Wong, E.S., Stewart, C.L., Burke, B., and Roux, K.J. (2013b). A mammalian KASH domain protein coupling meiotic chromosomes to the cytoskeleton. J Cell Biol *202*, 1023-1039.

Jahed, Z., Fadavi, D., Vu, U.T., Asgari, E., Luxton, G.W.G., and Mofrad, M.R.K. (2018). Molecular Insights into the Mechanisms of SUN1 Oligomerization in the Nuclear Envelope. Biophys J *114*, 1190-1203.

Jahed, Z., Shams, H., and Mofrad, M.R. (2015). A Disulfide Bond Is Required for the Transmission of Forces through SUN-KASH Complexes. Biophys J *109*, 501-509.

Kabsch, W. (2010). Xds. Acta Crystallogr D Biol Crystallogr *66*, 125-132.

Ketema, M., and Sonnenberg, A. (2011). Nesprin-3: a versatile connector between the nucleus and the cytoskeleton. Biochemical Society transactions *39*, 1719-1724.

Kumar, K.D., Gurusaran, M., Satheesh, S., Radha, P., Pavithra, S., Thulaa Tharshan, K., Helliwell, J.R., and Sekar, K. (2015). Online_DPI: a web server to calculate the diffraction precision index for a protein structure. Journal of applied crystallography *48*, 939-942.

Lee, C.Y., Horn, H.F., Stewart, C.L., Burke, B., Bolcun-Filas, E., Schimenti, J.C., Dresser, M.E., and Pezza, R.J. (2015). Mechanism and regulation of rapid telomere prophase movements in mouse meiotic chromosomes. Cell reports *11*, 551-563.
Lee, Y.L., and Burke, B. (2018). LINC complexes and nuclear positioning. Semin Cell Dev Biol *82*, 67-76.
Lei, K., Zhang, X., Ding, X., Guo, X., Chen, M., Zhu, B., Xu, T., Zhuang, Y., Xu, R., and Han, M. (2009). SUN1 and SUN2 play critical but partially redundant roles in anchoring nuclei in skeletal muscle cells in mice. Proc Natl Acad Sci U S A *106*, 10207-10212.
Lu, W., Gotzmann, J., Sironi, L., Jaeger, V.M., Schneider, M., Luke, Y., Uhlen, M., Szigyarto, C.A., Brachner, A., Ellenberg, J.*, et al.* (2008). Sun1 forms immobile macromolecular assemblies at the nuclear envelope. Biochim Biophys Acta *1783*, 2415-2426.
Luxton, G.W., Gomes, E.R., Folker, E.S., Vintinner, E., and Gundersen, G.G. (2010). Linear arrays of nuclear envelope proteins harness retrograde actin flow for nuclear movement. Science *329*, 956-959.
Madeira, F., Park, Y.M., Lee, J., Buso, N., Gur, T., Madhusoodanan, N., Basutkar, P., Tivey, A.R.N., Potter, S.C., Finn, R.D.*, et al.* (2019). The EMBL-EBI search and sequence analysis tools APIs in 2019. Nucleic Acids Res *47*, W636-W641.
McCoy, A.J., Grosse-Kunstleve, R.W., Adams, P.D., Winn, M.D., Storoni, L.C., and Read, R.J. (2007). Phaser crystallographic software. Journal of applied crystallography *40*, 658-674.
Meinke, P., Nguyen, T.D., and Wehnert, M.S. (2011). The LINC complex and human disease. Biochemical Society transactions *39*, 1693-1697.
Meinke, P., and Schirmer, E.C. (2015). LINC'ing form and function at the nuclear envelope. FEBS letters *589*, 2514-2521.
Mejat, A., and Misteli, T. (2010). LINC complexes in health and disease. Nucleus *1*, 40-52.
Morimoto, A., Shibuya, H., Zhu, X., Kim, J., Ishiguro, K., Han, M., and Watanabe, Y. (2012). A conserved KASH domain protein associates with telomeres, SUN1, and dynactin during mammalian meiosis. J Cell Biol *198*, 165-172.
P.V.Konarev, V.V.V., A.V.Sokolova, M.H.J.Koch, D. I. Svergun (2003). PRIMUS - a Windows-PC based system for small-angle scattering data analysis. J Appl Cryst *36*, 1277-1282
Panjkovich, A., and Svergun, D.I. (2016). Deciphering conformational transitions of proteins by small angle X-ray scattering and normal mode analysis. Physical chemistry chemical physics : PCCP *18*, 5707-5719.
Peranen, J., Rikkonen, M., Hyvonen, M., and Kaariainen, L. (1996). T7 vectors with modified T7lac promoter for expression of proteins in Escherichia coli. Anal Biochem *236*, 371-373.
Petoukhov, M.V., Franke, D., Shkumatov, A.V., Tria, G., Kikhney, A.G., Gajda, M., Gorba, C., Mertens, H.D., Konarev, P.V., and Svergun, D.I. (2012). New developments in the ATSAS program package for small-angle scattering data analysis. Journal of applied crystallography *45*, 342-350.
Roux, K.J., Crisp, M.L., Liu, Q., Kim, D., Kozlov, S., Stewart, C.L., and Burke, B. (2009). Nesprin 4 is an outer nuclear membrane protein that can induce kinesin-mediated cell polarization. Proc Natl Acad Sci U S A *106*, 2194-2199.
Sabel, C.E., Shepherd, J.L., and Siemann, S. (2009). A direct spectrophotometric method for the simultaneous determination of zinc and cobalt in metalloproteins using 4-(2-pyridylazo)resorcinol. Anal Biochem *391*, 74-76.
Shibuya, H., Ishiguro, K., and Watanabe, Y. (2014). The TRF1-binding protein TERB1 promotes chromosome movement and telomere rigidity in meiosis. Nature cell biology *16*, 145-156.
Sosa, B.A., Kutay, U., and Schwartz, T.U. (2013). Structural insights into LINC complexes. Curr Opin Struct Biol *23*, 285-291.
Sosa, B.A., Rothballer, A., Kutay, U., and Schwartz, T.U. (2012). LINC complexes form by binding of three KASH peptides to domain interfaces of trimeric SUN proteins. Cell *149*, 1035-1047.
Spindler, M.C., Redolfi, J., Helmprobst, F., Kollmannsberger, P., Stigloher, C., and Benavente, R. (2019). Electron tomography of mouse LINC complexes at meiotic telomere attachment sites with and without microtubules. Commun Biol *2*, 376.

Starr, D.A., and Fridolfsson, H.N. (2010). Interactions between nuclei and the cytoskeleton are mediated by SUN-KASH nuclear-envelope bridges. Annu Rev Cell Dev Biol *26*, 421-444.
Svergun D.I., B.C.K.M.H.J. (1995). CRYSOL – a Program to Evaluate X-ray Solution Scattering of Biological Macromolecules from Atomic Coordinates. J Appl Cryst *28*, 768-773.
Wang, W., Shi, Z., Jiao, S., Chen, C., Wang, H., Liu, G., Wang, Q., Zhao, Y., Greene, M.I., and Zhou, Z. (2012). Structural insights into SUN-KASH complexes across the nuclear envelope. Cell Res *22*, 1440-1452.
Waterhouse, A.M., Procter, J.B., Martin, D.M., Clamp, M., and Barton, G.J. (2009). Jalview Version 2--a multiple sequence alignment editor and analysis workbench. Bioinformatics *25*, 1189-1191.
Winter, G. (2010). xia2: an expert system for macromolecular crystallography data reduction. Journal of applied crystallography *43*, 186-190.
Zetka, M., Paouneskou, D., and Jantsch, V. (2020). "The nuclear envelope, a meiotic jack-of-all-trades". Curr Opin Cell Biol *64*, 34-42.
Zhang, X., Lei, K., Yuan, X., Wu, X., Zhuang, Y., Xu, T., Xu, R., and Han, M. (2009). SUN1/2 and Syne/Nesprin-1/2 complexes connect centrosome to the nucleus during neurogenesis and neuronal migration in mice. Neuron *64*, 173-187.
Zhou, Z., Du, X., Cai, Z., Song, X., Zhang, H., Mizuno, T., Suzuki, E., Yee, M.R., Berezov, A., Murali, R.*, et al.* (2012). Structure of Sad1-UNC84 homology (SUN) domain defines features of molecular bridge in nuclear envelope. J Biol Chem *287*, 5317-5326.

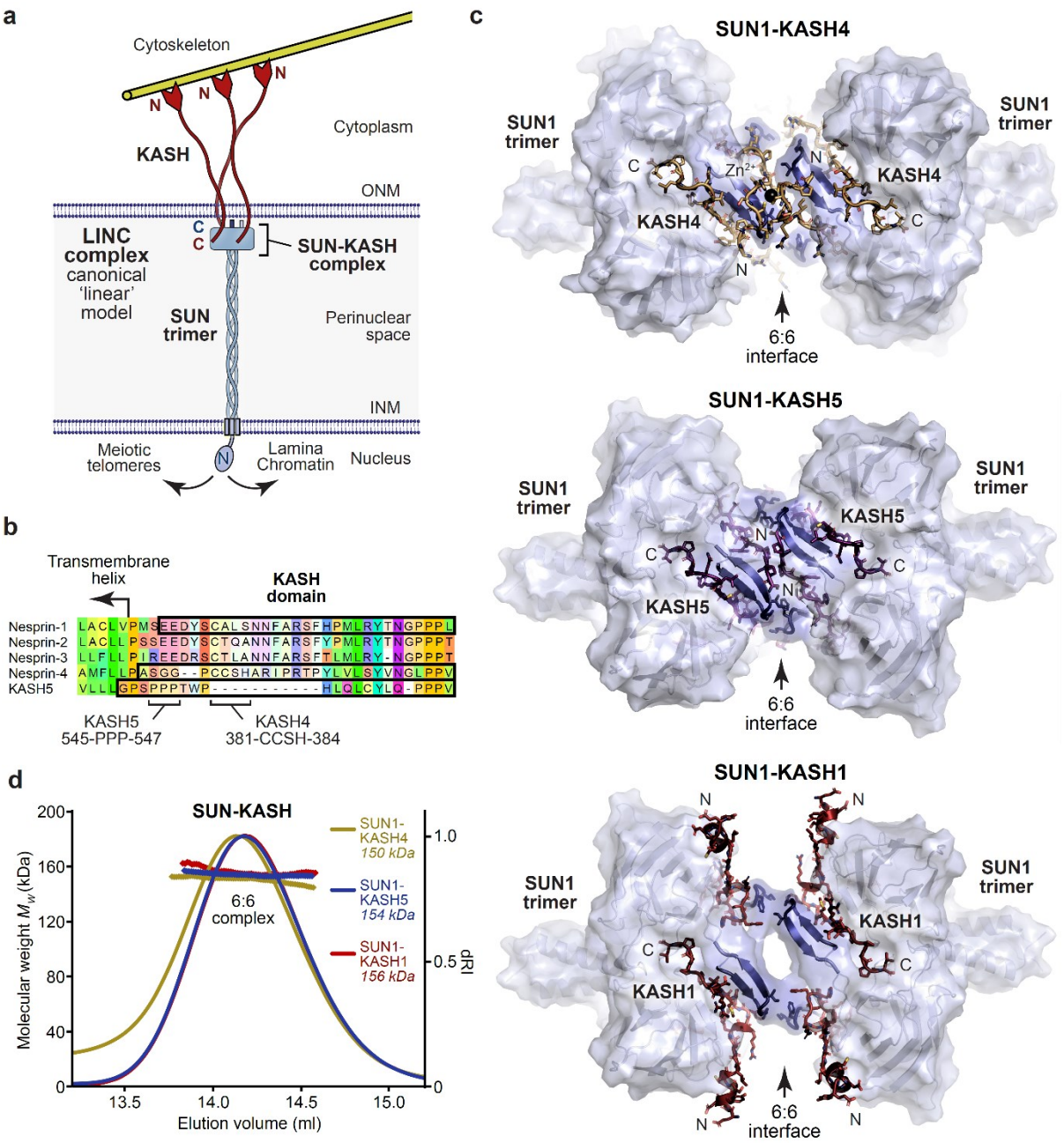

Figure 1

SUN-KASH complexes are 6:6 back-to-back assemblies.

(**a**) The LINC complex traverses the nuclear envelope to transmit forces between the cytoskeleton and nuclear components. The canonical model of the LINC complex is a linear structure formed of SUN and Nesprin proteins, which interact via a 3:3 complex between their SUN and KASH domains within the peri-nuclear space, and cross the inner and outer nuclear membranes (INM and ONM), respectively. (**b**) Sequence alignment of the KASH domains of human Nesprins 1-4 and KASH5, highlighting the

sequences used in this study (black outline), and indicating key amino-acids within KASH4 and KASH5 sequences. (**c**) Crystal structures of human SUN1-KASH4 (top), SUN1-KASH5 (middle) and SUN1-KASH1 (bottom). The SUN1 molecular surface is displayed with SUN1 KASH-lids highlighted in blue as cartoons, and KASH sequences are represented as sticks (yellow, purple and red, respectively). All structures are 6:6 complexes in which KASH proteins lie at the midline back-to-back interface between SUN1 trimers. (**d**) SEC-MALS analysis showing differential refractive index (dRI) profiles with fitted molecular weights (*Mw*) plotted as diamonds across elution peaks. SUN1-KASH4, SUN1-KASH5 and SUN1-KASH1 form 6:6 complexes in solution, with experimental molecular weights of 150 kDa, 154 kDa and 156 kDa, respectively (theoretical 6:6 – 155 kDa, 155 kDa and 157 kDa).

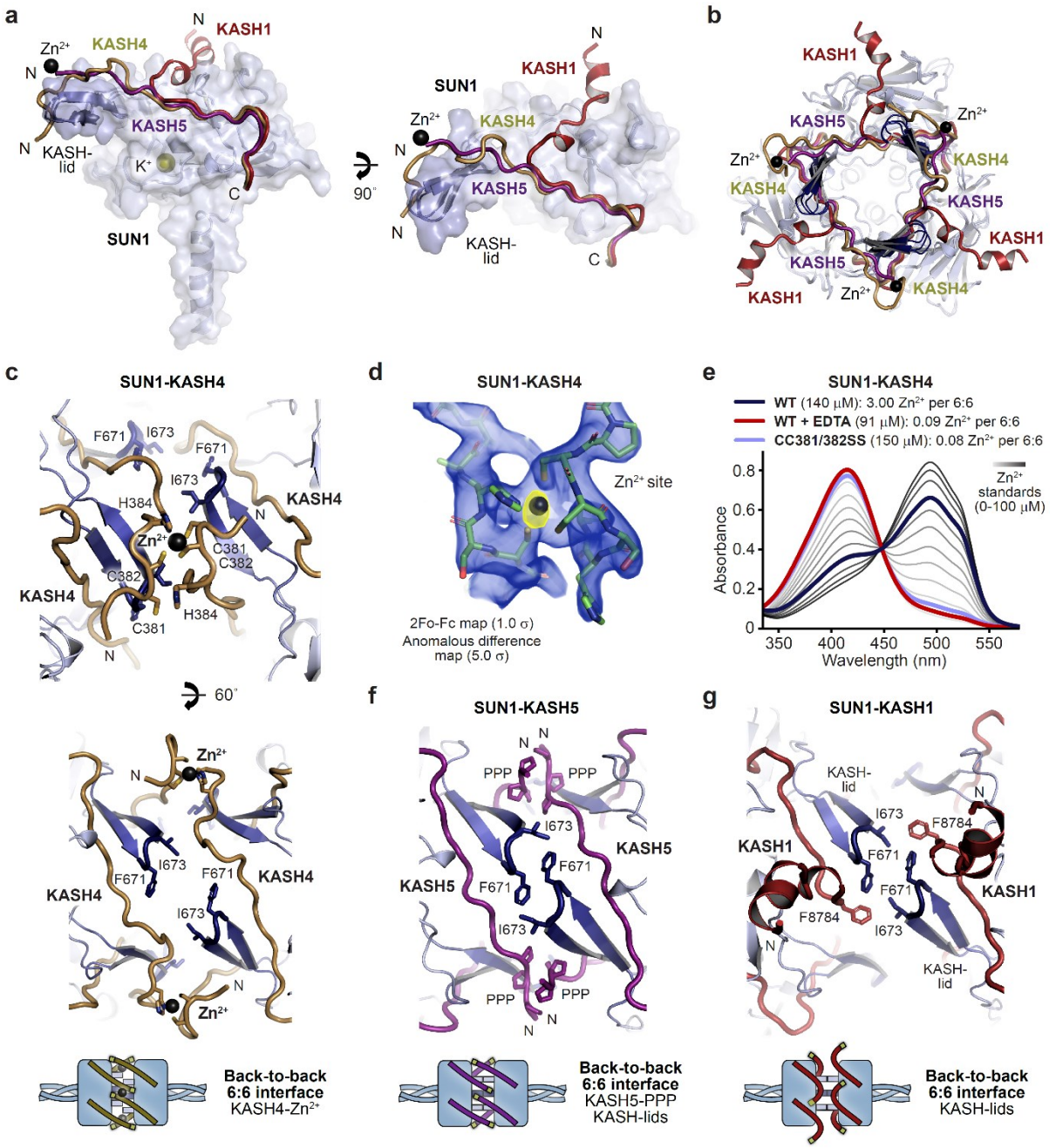

Figure 2

Specialised KASH sequences provide distinct SUN-KASH 6:6 assembly mechanisms.

(**a**) SUN-KASH 1:1 protomers from SUN1-KASH4, SUN1-KASH5 and SUN1-KASH1 crystal structures, superposed, and displayed as the SUN1 molecular surface with KASH-lids highlighted in blue as cartoons, and KASH sequences represented as cartoons (yellow, purple and red, respectively). (**b**) Cross-section through the back-to-back interface of superposed SUN1-KASH4, SUN1-KASH5 and SUN1-KASH1 6:6 assemblies such that their constituent 3:3 complexes are visible. (**c**) Structural details

of the SUN1-KASH4 6:6 interface, showing a zinc-binding site in which opposing KASH4 chains provide asymmetric ligands C381 and C382, and C382 and H384 (top), and the lack of interface-spanning interactions between opposing SUN1 KASH-lids (bottom). (**d**) 2Fo-Fc (blue) and anomalous difference (yellow) electron density maps contoured at 1.0 σ and 5.0 σ, respectively, at a zinc-binding site of SUN1-KASH4. (**e**) Spectrophotometric determination of zinc content for SUN1-KASH4 wild-type (dark blue; 3.00 Zn^{2+} per 6:6), wild-type with EDTA treatment prior to gel filtration (red; 0.09 Zn^{2+} per 6:6), and CC381/382SS (light blue; 0.08 Zn^{2+} per 6:6), using metallochromic indicator PAR, with zinc standards shown in a gradient from light to dark grey (0-100 µM). (**f**) Structural details of the SUN1-KASH5 6:6 interface, demonstrating interface-spanning interactions between PPP-motifs (amino-acids 545-PPP-547) of opposing KASH5 chains, and between amino-acids F671 and I673 of opposing SUN1 KASH-lids. (**g**) Structural details of the SUN1-KASH1 6:6 interface showing interactions between amino-acids F671 and I673 of opposing SUN1 KASH-lids that are supported by KASH1 amino-acid F8784, but with no interface-spanning interactions between opposing KASH1 chains.

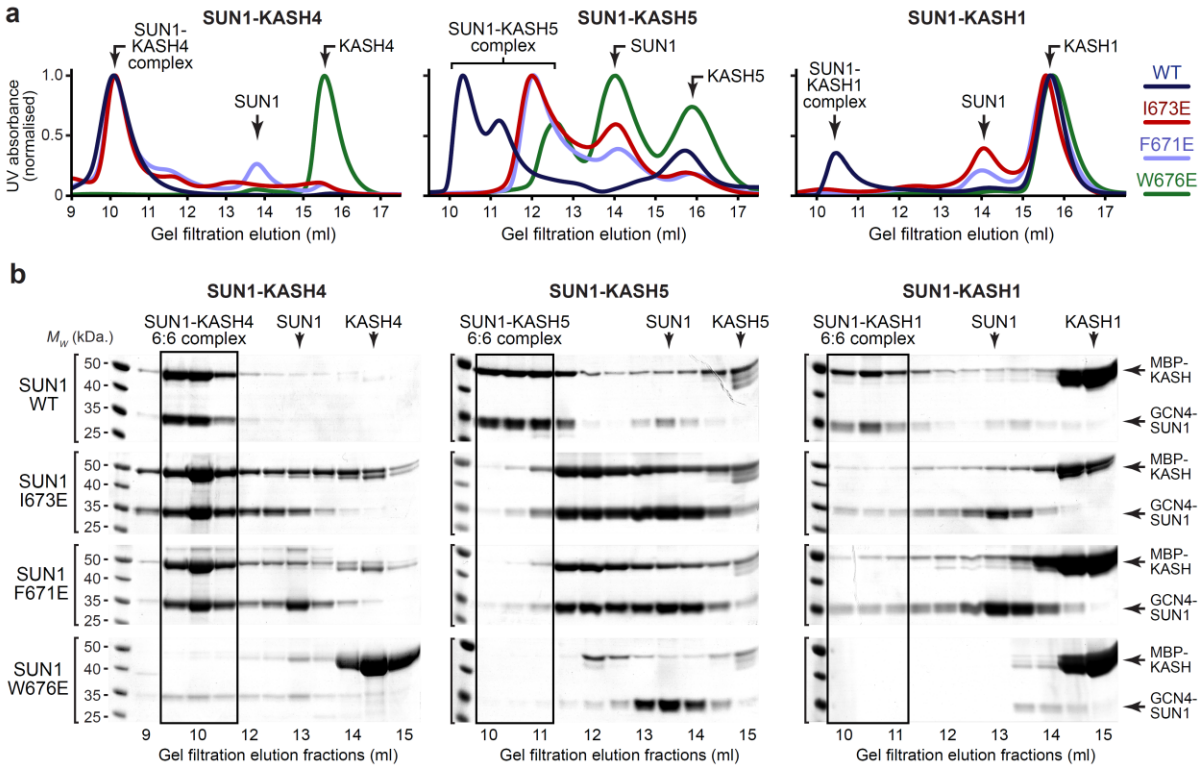

Figure 3

SUN1 KASH-lid residues involved in 6:6 assembly are essential for KASH1-binding.

(**a,b**) Gel filtration analysis of co-expressed and (co-)purified GCN4-SUN1 and MBP-KASH. (**a**) Gel filtration chromatograms (UV absorbance at 280 nm) across elution profiles for SUN1 wild-type (WT; dark blue), I673E (red), F671E (light blue) and W676E (green), with KASH4 (left), KASH5 (middle) and KASH1 (right), and (**b**) SDS-PAGE of their corresponding elution fractions.

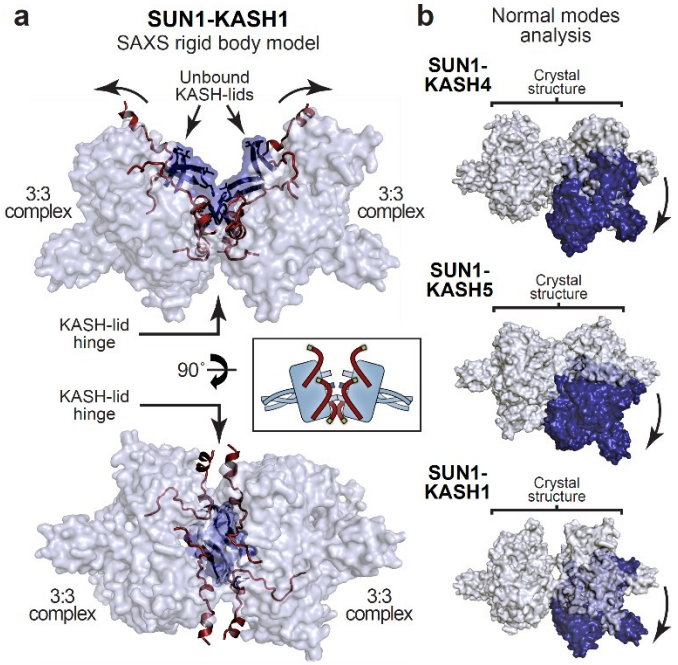

Figure 4

Hinge-link conformational flexibility within SUN-KASH 6:6 assemblies.

(**a**) SAXS rigid body model of SUN1-KASH1 in which two constituent 3:3 complexes from its crystal structure were assigned as rigid bodies, with the 6:6 assembly generated by fitting to experimental SAXS data of solution SUN1-KASH1 (χ^2 = 1.56). (**b**) Normal mode analysis of SUN-KASH complexes in which non-linear normal modes calculated by the NOLB algorithm are shown as the largest amplitude of motion of one constituent 3:3 complex (blue) relative to its original position and its stationary opposing 3:3 complex within the crystal structure (grey) for SUN1-KASH4 (top), SUN1-KASH5 (middle) and SUN1-KASH1 (bottom).

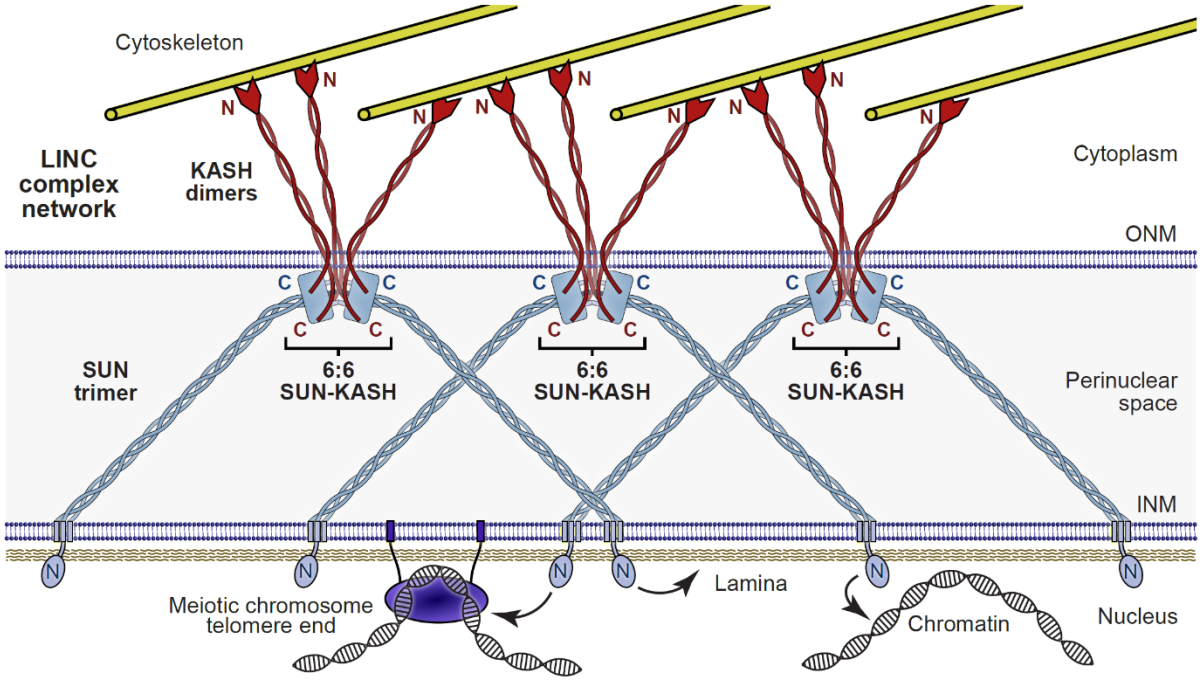

Figure 5

The LINC complex as a branched network of SUN-KASH assemblies.

Model of the LINC complex as a branched network in which SUN-KASH 6:6 complexes act as nodes for force integration and distribution between two SUN trimers and three KASH dimers, which can bind to spatially-separated and distinct nuclear and cytoskeletal components, respectively. This model enables cooperation between adjacent molecules within a LINC complex network to facilitate the transduction of large and coordinated forces across the nuclear envelope.

Table 1 Data collection, phasing and refinement statistics

	SUN1-KASH4	SUN1-KASH5	SUN1-KASH1
PDB accession	6R16	6R2I	6R15
Data collection			
Space group	$P2_12_12_1$	$P6_322$	$P6_322$
Cell dimensions			
a, *b*, *c* (Å)	104.37, 117.21, 138.42	80.16, 80.16, 177.62	80.45, 80.45, 182.55
α, β, γ (°)	90.00, 90.00, 90.00	90.00, 90.00, 120.00	90.00, 90.00, 120.00
Wavelength (Å)	0.9795	0.9282	0.9282
Resolution (Å)	48.83 – 2.75 (2.85 – 2.75)[a]	88.81 – 1.54 (1.57 – 1.54)[a]	65.09 – 1.82 (1.87 – 1.82)[a]
R_{meas}	0.111 (1.355)	0.070 (1.551)	0.085 (2.192)
R_{pim}	0.056 (0.741)	0.015 (0.329)	0.019 (0.465)
Completeness (%)	99.7 (97.5)	97.5 (100.0)	100.0 (100.0)
$I/\sigma(I)$	15.4 (1.4)	23.5 (2.2)	21.5 (1.7)
$CC_{1/2}$	0.999 (0.488)	1.000 (0.801)	1.000 (0.776)
Multiplicity	7.1 (5.6)	21.3 (22.1)	20.6 (21.9)
Refinement			
Resolution (Å)	47.67 – 2.75	23.99 – 1.54	65.09 – 1.82
No. reflections	44658	49372	32230
R_{work} / R_{free}	0.2190/0.2549	0.1495/0.1683	0.1587/0.1817
Cruickshank DPI (Å)	0.25	0.06	0.06
No. atoms	10562	2127	2107
Protein	10451	1817	1845
Ligand/ion	21	1	26
Water	90	309	236
B factors	80.64	36.45	48.87
Protein	80.87	35.09	47.73
Ligand/ion	68.03	18.87	119.12
Water	56.37	44.50	50.06
R.m.s deviations			
Bond lengths (Å)	0.002	0.011	0.013
Bond angles (°)	0.444	1.076	0.995

[a]Values in parentheses are for highest-resolution shell.

Table 2 Summary of SEC-SAXS data

	SUN1 I673E (monomer)	**SUN1-KASH4 (6:6)**	**SUN1-KASH1 (6:6)**	**SUN1-KASH5 (6:6)**
Guinier analysis				
I(0) (cm^{-1})	0.042	0.045	0.130	0.010
Rg (Å)	21	40	39	38
q_{min} ($Å^{-1}$)	0.0080	0.0014	0.0090	0.0070
***P(r)* analysis**				
I(0) (cm^{-1})	0.042	0.045	0.132	0.10
Rg (Å)	22	40	39	39
D_{max} (Å)	82	135	130	135
Porod volume ($Å^3$)	39367	292301	303602	274824
MW from Porod volume (kDa)	23	172	179	162
V_C ($Å^2$)	238	825	853	784
MW from V_C (kDa)	22	139	152	131
DAMMIF ab initio modelling (30 models)				
Symmetry	P1	N/A	N/A	N/A
NSD mean	0.645	N/A	N/A	N/A
χ^2 (reference model)	1.85	N/A	N/A	N/A
Structural modelling				
CRYSOL - crystal structure (χ^2)	5.43	1.62	4.83	5.50
CORAL - modelling of N-termini (χ^2)	N/A	1.25	4.55	1.70
CORAL - rigid body modelling (χ^2)	N/A	N/A	1.56	N/A
SREFLEX - normal mode analysis (χ^2)	1.72 – 1.98	N/A	N/A	N/A

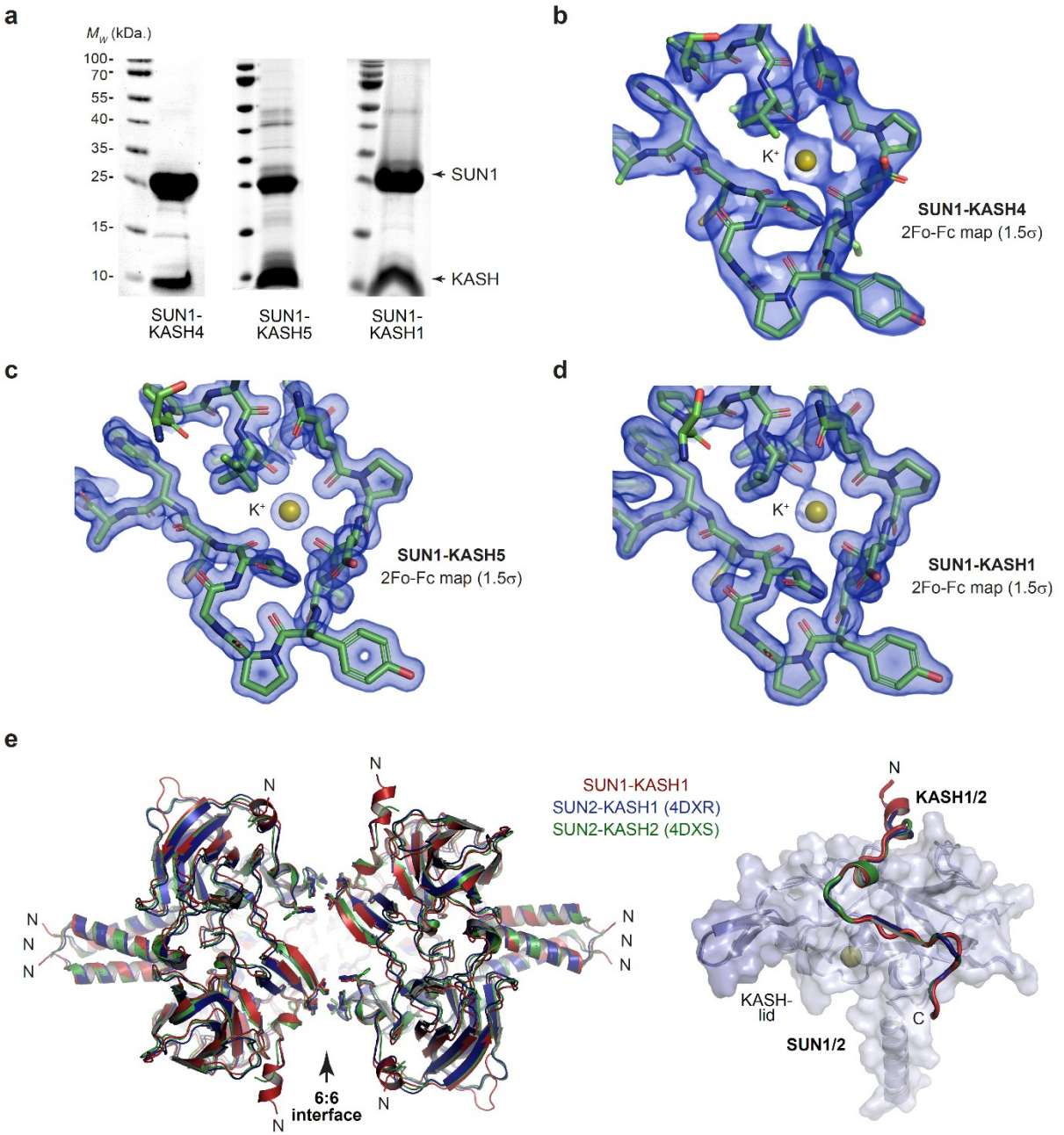

Supplementary Figure 1

Crystal structures of SUN-KASH complexes.

(**a**) SDS-PAGE of purified SUN1-KASH4 (left), SUN1-KASH5 (middle) and SUN1-KASH1 (right) complexes used for crystallographic and biophysical experiments. (**b-d**) 2Fo-Fc electron density maps contoured at 1.5 σ of the same orientation of the SUN1 K^+-binding site for (**b**) SUN1-KASH4, (**c**) SUN1-KASH5 and (**d**) SUN1-KASH1. (**e**) Superposition of SUN1-KASH1 (red) with SUN2-KASH1 (blue; PDB accession 4DXR) and SUN2-KASH2 (green; PDB accession 4DXS) (Sosa et al., 2012), showing the common 6:6 assembly that is present within their crystal lattices (left) and their constituent 1:1 protomers (right).

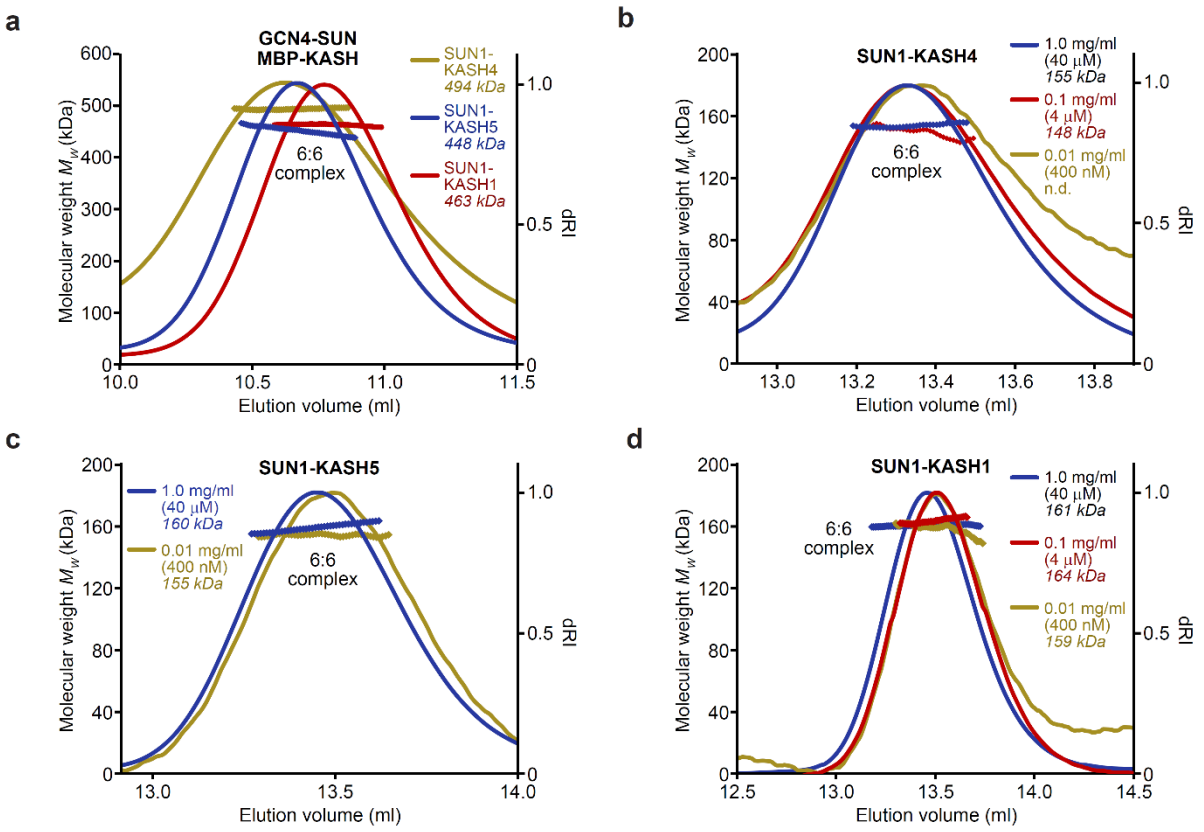

Supplementary Figure 2

SUN-KASH complexes are 6:6 assemblies.

(**a-d**) SEC-MALS analysis. (**a**) GCN4-SUN1 and MBP-KASH form 6:6 complexes of 494 kDa (KASH4, yellow), 448 kDa (KASH5, blue) and 463 kDa (KASH1, red) (theoretical 6:6 – 464 kDa, 464 kDa and 466 kDa). (**b-c**) Dilution series of SUN-KASH complexes analysed at 1.0 mg/ml (blue), 0.1 mg/ml (red) and 0.01 mg/ml (yellow) for (**b**) SUN1-KASH4 (theoretical 6:6 - 155 kDa), (**c**) SUN1-KASH5 (theoretical 6:6 - 155 kDa) and (**d**) SUN1-KASH1 (theoretical 6:6 - 157 kDa).

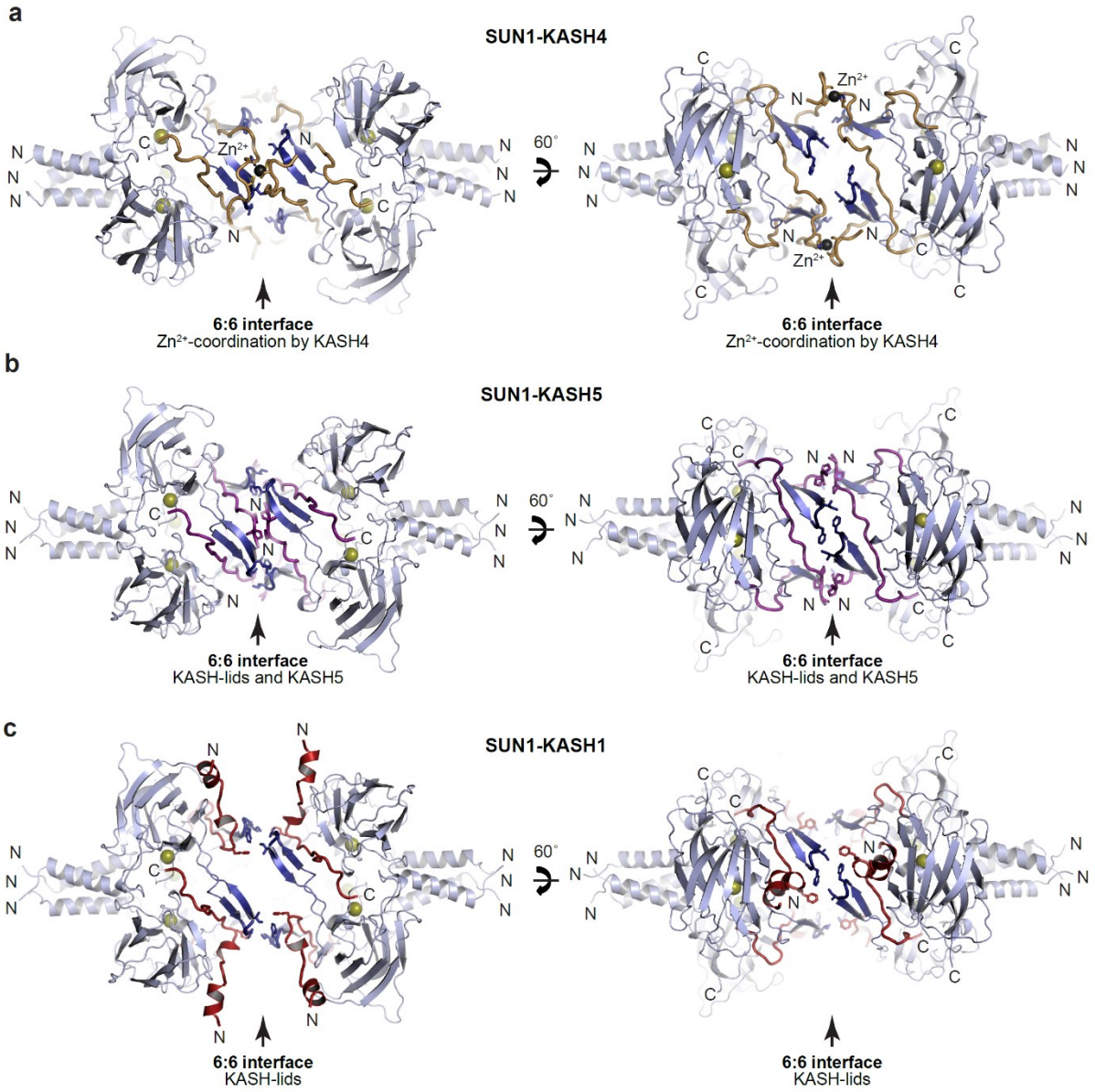

Supplementary Figure 3

SUN-KASH crystal structures.

(**a-c**) Crystal structures of (**a**) SUN1-KASH4, (**b**) SUN1-KASH5 and (**c**) SUN1-KASH1 shown in cartoon representation with SUN1 KASH-lids highlighted in blue and KASH4, KASH5 and KASH1 shown in yellow, purple and red, respectively.

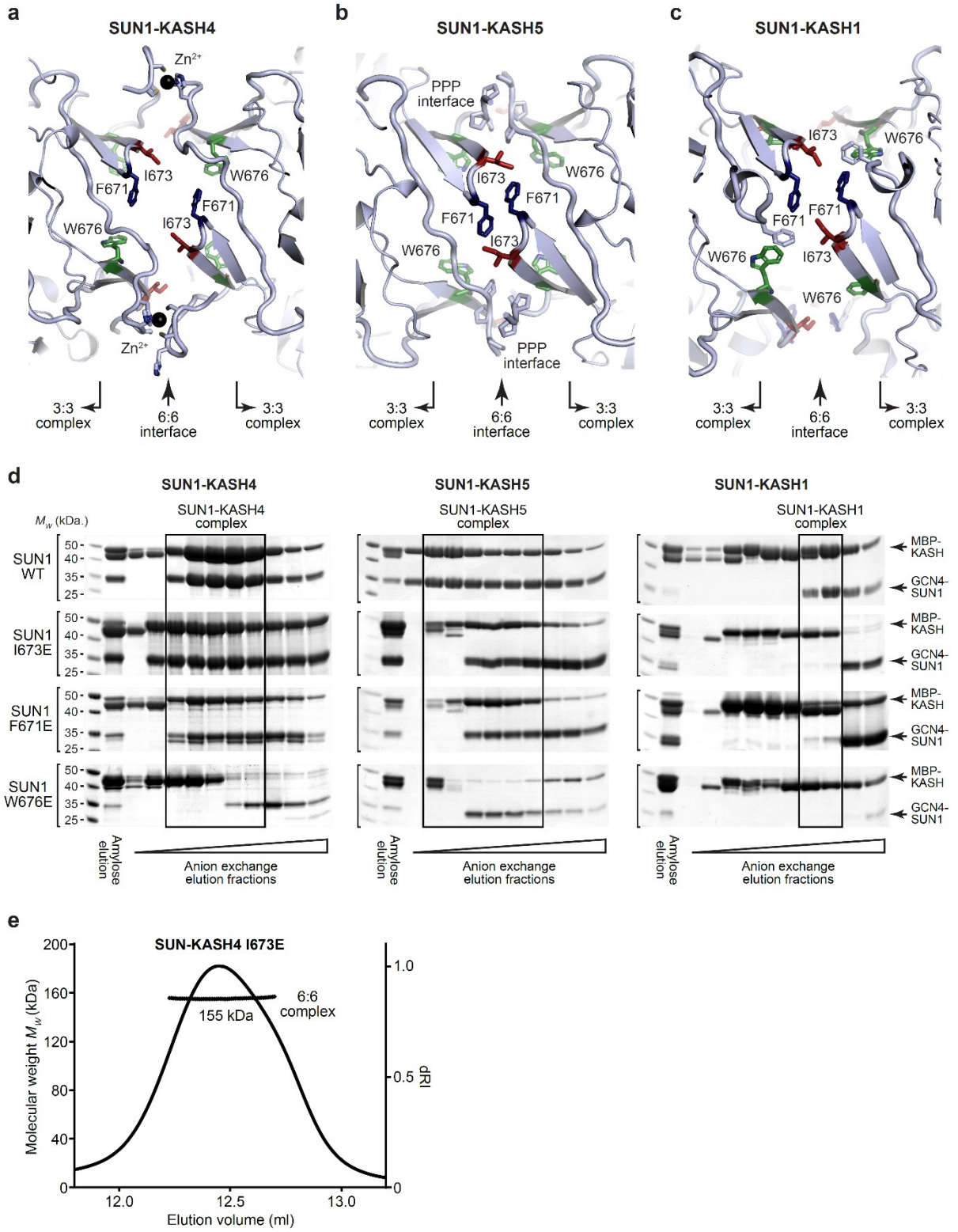

Supplementary Figure 4

SUN-KASH complex formation upon SUN1 KASH-lid mutagenesis.

(**a-c**) Structural details of the 6:6 interface of (**a**) SUN1-KASH4, (**b**) SUN1-KASH5 and (**c**) SUN1-KASH1, highlighting SUN1 KASH-lid residues I673 (red), F671 (blue) and W676 (green). (**d**) SDS-PAGE of anion

exchange elution profiles of co-expressed and (co-)purified GCN4-SUN1 and MBP-KASH, comprising SUN1 wild-type, I673E, F671E and W676E, with KASH4 (left), KASH5 (middle) and KASH1 (right). (**e**) SEC-MALS analysis demonstrating that SUN1 I673E and KASH4 form a 155 kDa 6:6 complex (theoretical 6:6 - 155 kDa).

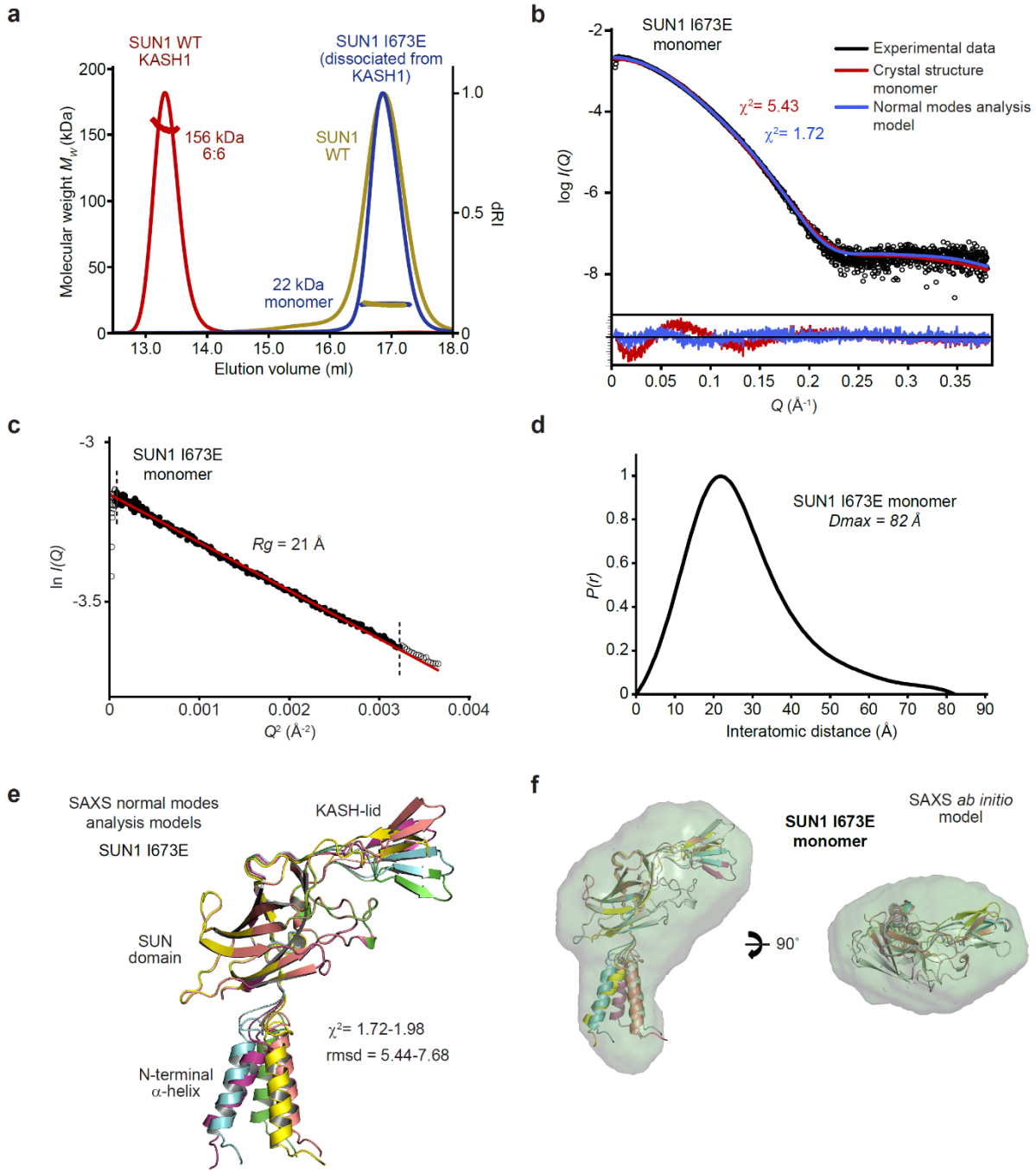

Supplementary Figure 5

SUN1 I673E dissociates from KASH1 as a structurally-intact monomer.

(**a**) SEC-MALS analysis demonstrating that isolated SUN1 wild-type (WT; yellow), and SUN1 I673E that has dissociated following co-expression with KASH1 (blue), are 22 kDa monomers (theoretical – 23 kDa). The wild-type SUN1-KASH1 6:6 complex is shown in red for comparison. (**b-f**) SAXS analysis of the SUN1 I673E monomer. (**b**) SAXS scattering curve overlaid with theoretical scattering curves of a SUN1 protomer from the SUN1-KASH1 crystal structure (red; χ^2 = 5.43) and its normal mode analysis

model (blue; χ^2 = 1.72). (**c**) SAXS Guinier analysis revealing a radius of gyration (*Rg*) of 21 Å; the linear fit is shown in black and demarcated by dashed vertical lines (Q.Rg values were < 1.3). (**d**) SAXS *P(r)* distribution showing a maximum dimension of 82 Å. (**e**) SAXS normal mode analysis in which the five highest scoring models are displayed, based on their fit to the experimental SAXS data (χ^2 = 1.72-1.98), and demonstrate hinge-like motion of the N-terminal α-helix relative to the SUN domain. (**e**) SAXS *ab initio* model (NSD = 0.645; reference model χ^2 = 1.85) into which the normal mode analysis models are docked.

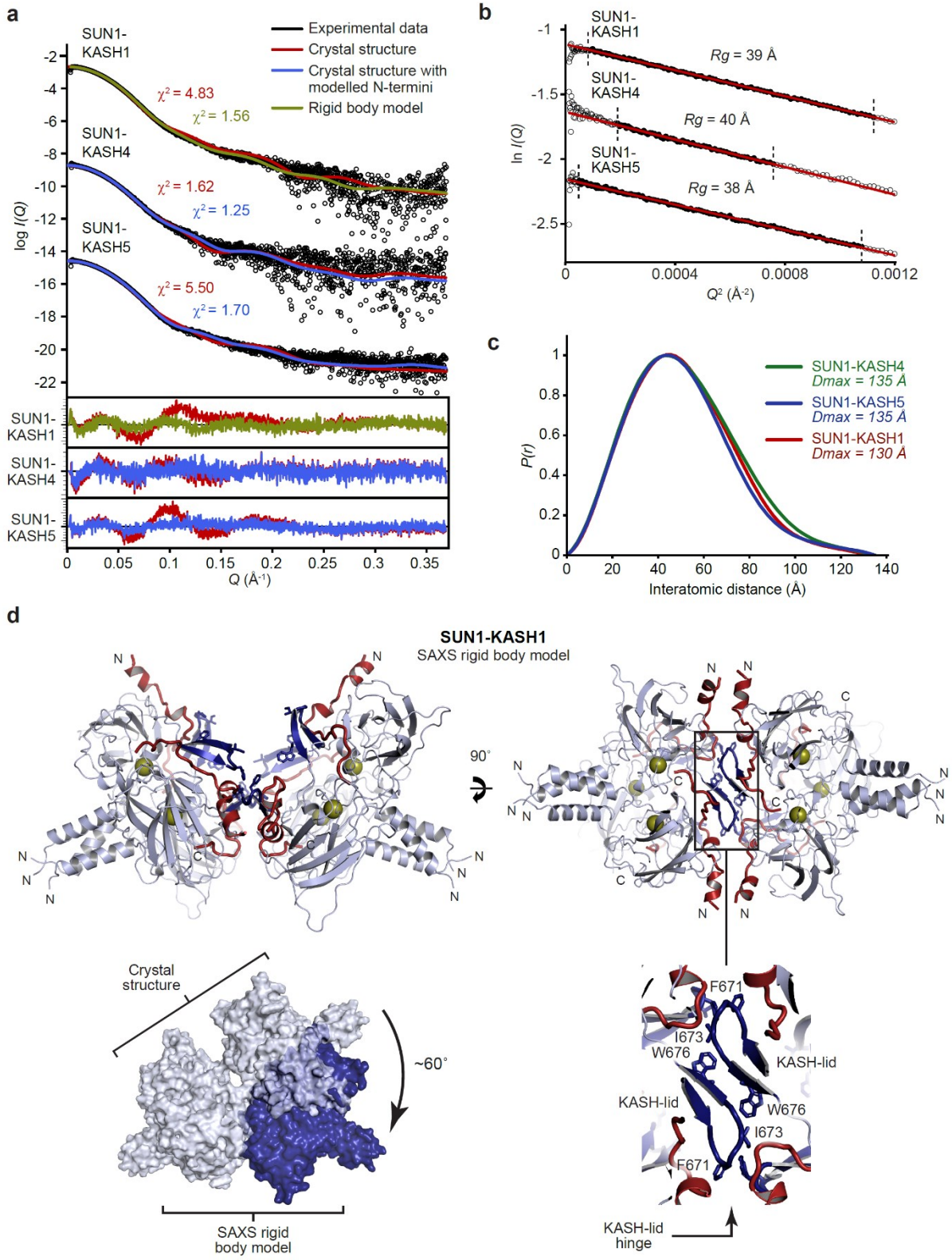

Supplementary Figure 6

SAXS analysis of SUN-KASH complexes.

(**a**) SAXS scattering curves of SUN1-KASH4, SUN1-KASH5 and SUN1-KASH1 overlaid with theoretical scattering curves of their crystal structures (red), crystal structures with KASH flexible N-termini

modelled by CORAL (blue) and rigid body model of two 3:3 complexes (yellow). Residuals for each fit are shown (inset). (**b**) SAXS Guinier analysis revealing radius of gyration (*Rg*) values of 38 Å, 40 Å and 39 Å, respectively; the linear fits are shown in black and demarcated by dashed vertical lines (*Q.Rg* values were < 1.3). (**c**) SAXS *P(r)* distributions showing maximum dimensions of 135 Å, 135 Å and 130 Å, respectively. (**d**) SAXS rigid body model of SUN1-KASH1 shown in cartoon representation, highlighting the structural details of the predicted KASH-lid interface, alongside a surface representation of the approximately 60˚ motion of one constituent 3:3 complex (blue) relative to its original position and its stationary opposing 3:3 complex within the crystal structure (grey).